

Supporting Information

A dual-response fluorescent probe Rh-O-QL for simultaneous monitoring NAD(P)H and pH during mitochondrial autophagy

Liandi Guan^{a, b}, Wanting Hu^b, Shiyu Zhang^b, Yongjian Ai^b, Qionglin Liang^{*b}

^a Institute of Basalt Fiber in Eco-Application, School of Environmental Science and Engineering, Qingdao University, Qingdao, Shandong, 266071, PR China

^b MOE Key Laboratory of Bioorganic Phosphorus Chemistry & Chemical Biology, Department of Chemistry, Laboratory of Flexible Electronics Technology, Center for Synthetic and Systems Biology, Tsinghua University, Beijing 100084, P.R. China

Experimental	3
Materials and Chemicals	3
Apparatus	3
Synthesis of Rh-O-Q	3
Synthesis of Rh-O-QL	4
Synthesis of Rh-OH	4
<i>In Vitro</i> Detection of NAD(P)H	5
Measurement of pka of Rh-OH	5
Fluorescence characteristics of Rh-OH responding to pH	6
Cell Culture and Cytotoxicity Test	7
Fluorescence Imaging in living cells	7
Scheme S1. Design of dual-response near-infrared dye molecule Rh-O-QL	8
Scheme S2. Proposed mechanism of probe Rh-O-QL response to NAD(P)H	8
Figure S1. ¹ H NMR spectra of compound Rh-OH	9
Figure S2. ¹³ C NMR spectra of compound Rh-OH	9
Figure S3. ¹³ C NMR spectra of compound Rh-O-QL	10
Figure S4. ESI-MS spectra of compound Rh-O-QL	10
Figure S5. PH-responsive photophysical properties of Rh-OH	11
Figure S6. Chromaticity diagram of Rh-OH at different pH conditions	11
Figure S7. Fluorescence properties of acid-base configuration of Rh-OH	12
Figure S8. Time-dependent UV-vis absorption spectrum changes of Rh-DD-QL with NAD(P)H	12
Figure S9. Line profile analysis for fluorescence intensity changes of Rh-O-QL with NAD(P)H	13
Figure S10. Relative fluorescence intensity of 20 μM Rh-O-QL in the presence of various analytes	13
Figure S11. HPLC-MS spectrogram of Rh-O-QL before and after the addition of NAD(P)H	14
Figure S12. Relative abundance of Rh-O-QL and Rh-OH after incubation with different equivalents NAD(P)H	15
Figure S13. Chemical structures and TDDFT analysis of Rh-O-QL, Rh-OH, and Rh-O ⁻	15
Table S1. DFT calculation results of Rh-O-QL, Rh-OH, and Rh-O ⁻	15
Figure S14. Cytotoxicity Assays of probe Rh-O-QL	16
Figure S15. The time-dependence of cellular fluorescence images and the fluorescence intensity of 4T1 cells	16
Figure S16. Fluorescence images of exogenous NAD(P)H in 4T1 cells	16
Figure S17. Fluorescence images of exogenous glucose in 4T1 cells	17
Reference	17

Experimental

Materials and Chemicals

All the reagents and chemicals in the analytical grade were purchased from commercial suppliers and used without further purification. Beta-NAD(P)H, Beta-NAD(P)⁺, ATP, ADP, 3-bromomethylquinoline, and 4-Hydroxybenzaldehyde were purchased from Bide Pharmatech Ltd. (Shanghai, China). 4-diethylaminoketonic acid, cyclohexanone, and methyl iodide (CH₃I) were obtained from Energy Chemical. Cell culture media DMEM was obtained from Thermo Fisher Technology Co., Ltd (Shanghai, China). Mito-Tracker Green FM (50 μL) was purchased from Shanghai Yuanye Bio-Technology Co., Ltd (Shanghai, China). Lyso-Tracker Green (50 μL) was purchased from Beyotime Biotechnology Co., Ltd. Reagents used for HPLC-MS detection were HPLC-MS grade. The cell culture dishes were purchased from NEST Biotechnology (Wuxi, China). All chemicals were used as received without further purification.

Apparatus

¹H NMR spectra were collected on a JNM-ECA400 NMR system or JNM-ECS600 NMR system (JEOL, Japan), and tetramethyl silane (TMS) was used as the internal standard. Mass spectral data were recorded on Q Exactive Orbitrap Mass Spectrometers (Thermo Fisher, USA). UV-vis absorption spectra were recorded on a UV-6100 ultraviolet spectrophotometer (Shanghai Meiputa instrument Co., Ltd) and an EnVision Multilabel Reader (PerkinElmer, USA), and fluorescence spectra were performed on a FluoroMax fluorescence spectrometer (HORIBA Scientific, French) with a 1 cm³ standard quartz cell. Confocal imaging was conducted with a Leica TCS SP8 STED ultrahigh resolution confocal microscope (Leica, Germany).

Synthesis of Rh-O-Q

3-bromomethylquinoline (2.0 mmol), 4-Hydroxybenzaldehyde (2.2 mmol), and K₂CO₃ (3.0 eq.) were mixed in DMF (4.0 mL). The mixture was stirred at 70°C for 4.0 h in a N₂ atmosphere. TLC showed the reaction was complete. The mixture was filtered to remove K₂CO₃ residue and extracted with chloroform to collect the organic layer, which was washed with water following dilute HCl and dried with MgSO₄ before concentrated. The crude product was dissolved in chloroform, and purified by recrystallization with anhydrous ether to obtain 360 mg yellow solid (yield 68%).

H1 was synthesized according to the method reported before.[1] The compound H1 (1 mmol) and HO-QL (1.2 eq.) were dissolved in 10.0 mL acetic anhydride, and the mixture was stirred at 90°C for 12.0 h in a N₂ atmosphere. TLC showed the reaction was complete. The solvent acetic anhydride was removed under

reduced pressure, and the obtained solid was purified by silica gel chromatography ($\text{CH}_2\text{Cl}_2/\text{CH}_3\text{CH}_2\text{OH} = 20:1$) to get a purple solid product (410 mg, yield: 68%). ^1H NMR (400 MHz, $\text{DMSO}-d_6$) δ 9.01 (d, $J = 2.2$ Hz, 1H), 8.45 (d, $J = 2.1$ Hz, 1H), 8.06 - 8.01 (m, 2H), 7.98 - 7.90 (m, 2H), 7.81 - 7.74 (m, 2H), 7.68 - 7.63 (m, 2H), 7.45 - 7.39 (m, 2H), 7.34 - 7.30 (m, 3H), 7.16 - 7.11 (m, 2H), 6.52 (d, $J = 2.5$ Hz, 1H), 6.42 (d, $J = 2.5$ Hz, 1H), 6.39 (s, 1H), 5.39 (s, 2H), 3.38 - 3.34 (m, 4H), 2.89 (s, 1H), 2.73 (s, 1H), 1.54 (d, $J = 15.9$ Hz, 4H), 1.09 (t, $J = 7.0$ Hz, 6H). HR-MS: calc. $[\text{C}_{41}\text{H}_{37}\text{N}_2\text{O}_4]^+$: 621.2748, found: 621.2745.

Synthesis of Rh-O-QL

The compound Rh-O-Q (0.5 mmol) was dissolved in 4.0 mL anhydrous CH_2Cl_2 , followed by adding dropwise CH_3I (5.0 eq.). The solution was stirred at 35°C for 48.0 h. After the solvent was removed under reduced pressure, the crude product was washed with cyclohexane and purified by silica gel chromatography ($\text{CH}_2\text{Cl}_2/\text{CH}_3\text{CH}_2\text{OH} = 15:1$) to get a black solid product (50 mg, yield: 16%). ^1H NMR (600 MHz, $\text{DMSO}-d_6$) δ 8.97 (d, $J = 2.2$ Hz, 1H), 8.41 (d, $J = 2.2$ Hz, 1H), 8.01 (d, $J = 8.4$ Hz, 1H), 7.98 (dd, $J = 8.2, 1.4$ Hz, 1H), 7.90 (d, $J = 7.7$ Hz, 1H), 7.76 - 7.72 (m, 2H), 7.63 (t, $J = 7.6$ Hz, 1H), 7.60 (t, $J = 7.4$ Hz, 1H), 7.38 (d, $J = 8.5$ Hz, 2H), 7.30 (s, 1H), 7.26 (d, $J = 7.8$ Hz, 1H), 7.09 (d, $J = 8.6$ Hz, 2H), 6.48 (d, $J = 2.5$ Hz, 1H), 6.38 (dd, $J = 9.0, 2.6$ Hz, 1H), 6.34 (d, $J = 8.9$ Hz, 1H), 5.34 (s, 2H), 3.34 (s, 3H), 3.29 (d, $J = 7.0$ Hz, 4H), 2.73 - 2.66 (m, 1H), 2.58 - 2.50 (m, 1H), 1.84 - 1.75 (m, 1H), 1.59 - 1.46 (m, 3H), 1.04 (t, $J = 7.0$ Hz, 6H). ^{13}C NMR (150 MHz, $\text{DMSO}-D_6$) δ 169.62, 157.83, 152.24, 152.20, 151.13, 149.50, 147.76, 146.91, 135.82, 135.21, 131.45, 130.59, 130.40, 130.23, 129.96, 129.31, 128.92, 128.74, 128.67, 127.87, 127.51, 127.24, 125.09, 124.11, 115.32, 109.37, 107.58, 104.66, 97.32, 86.48, 67.73, 44.21, 44.06, 27.16, 23.09, 22.45, 12.91. HR-MS: calc. Rh-O-QL $[\text{C}_{42}\text{H}_{40}\text{NO}_4]^{2+}$: 318.1489, found: 318.1484.

Synthesis of Rh-OH

The compound H1 (1 mmol) and 4-Hydroxybenzaldehyde (1.2 eq.) were dissolved in 10.0 mL acetic acid, and the mixture was stirred at 90°C for 12.0 h in a N_2 atmosphere. TLC showed the reaction was complete. The solvent acetic acid was removed under reduced pressure, and the obtained solid was purified by silica gel chromatography ($\text{CH}_2\text{Cl}_2/\text{CH}_3\text{CH}_2\text{OH} = 15:1$) to get a purple solid product (360 mg, yield: 75%). ^1H NMR (600 MHz, $\text{DMSO}-d_6$) δ 7.90 (d, $J = 7.7$ Hz, 1H), 7.71 (t, $J = 7.5$ Hz, 1H), 7.61 (t, $J = 7.5$ Hz, 1H), 7.30 (s, 1H), 7.25 (t, $J = 7.2$ Hz, 3H), 6.71 (d, $J = 8.2$ Hz, 2H), 6.49 (d, $J = 2.7$ Hz, 1H), 6.40 (dd, $J = 9.1, 2.6$ Hz, 1H), 6.35 (d, $J = 8.9$ Hz, 1H), 3.31 (d, $J = 7.1$ Hz, 4H), 2.72 - 2.68 (m, 1H), 2.37 - 2.53 (m, 1H), 1.86 - 1.77 (m, 1H), 1.57 - 1.51 (m, 3H), 1.05 (t, $J = 7.0$ Hz, 6H). ^{13}C NMR (150 MHz, $\text{DMSO}-D_6$) δ 169.68, 152.49, 149.61, 135.26, 132.10, 130.21, 128.71, 127.13, 126.45, 125.54, 124.48, 116.53, 109.46, 108.01, 105.43, 97.25, 44.24, 27.32, 23.39, 22.40, 12.93. HR-MS: calc. Rh-OH $[\text{C}_{31}\text{H}_{30}\text{NO}_4]^+$: 480.2170, found: 480.2168.

***In Vitro* Detection of NAD(P)H**

Rh-O-QL stock solution (2 mM) was prepared by dissolving Rh-O-QL in solvent (H₂O/DMSO = 8:2). For all experiments, the stock solution of Rh-O-QL was diluted with Tris-HCl buffer solution (Tris-HCl, 0.01 M, pH = 6, 7, and 8) to give a work solution of a Tris-HCl buffer (0.01 M, pH 6, 7, and 8, 0.2% DMSO) containing 20 μM Rh-O-QL. Stock solution of NAD(P)H and various interfering reagents were prepared in water and added to the solution of Rh-O-QL (20 μM). The time-depending spectral test started immediately after adding NAD(P)H within 0-60 min. The concentration-depending spectrum was recorded after incubation of Rh-O-QL and NAD(P)H at 37°C for 1.0 h. The UV-vis spectra were collected from 400 nm to 750 nm, and the fluorescence spectra were recorded ($\lambda_{\text{ex}} = 600$ nm), where slit widths were 10/10 nm.

Measurement of pka of Rh-OH

Considering the fluorescent group Rh-OH as a monoprotic weak acid (HB), it exhibits the following dissociation equilibrium under different pH conditions:

$$[\text{HB}] = [\text{B}^-] + [\text{H}^+] \quad (\text{Eq. S1})$$

At any pHs, the Rh-OH concentration (c) is the sum of the acidic HB and basic B⁻ concentrations:

$$c = [\text{HB}] + [\text{B}^-] \quad (\text{Eq. S2})$$

Therefore, the dissociation coefficient of Rh-OH is as follows:

$$K_a = \frac{[\text{H}^+][\text{B}^-]}{[\text{HB}]} \quad (\text{Eq. S3})$$

According to Lambert Beer's law, the absorption of Rh-OH is as follows:

$$A = \varepsilon_{\text{HB}}b[\text{HB}] + \varepsilon_{\text{B}^-}b[\text{B}^-] \quad (\text{Eq. S4})$$

Among them, A , ε_{HB} , ε_{B^-} , and b represent absorption intensity, molar absorption coefficient of HB, molar absorption coefficient of B⁻, and optical path length, respectively.

Selecting 565 nm, which is the maximum absorption of HB, as wavelength 1, and 671 nm, which is equal to the absorption of HB at 565 nm in B⁻, as wavelength 2. By using dual wavelength spectrophotometry, the following can be obtained:

$$A_{565} - A_{671} = \varepsilon_{\text{HB}_{565}}b[\text{HB}] - \varepsilon_{\text{HB}_{671}}b[\text{HB}] \quad (\text{Eq. S5})$$

Substituting Eq. S1 and S2 into Eq. S5, the following results were obtained:

$$Y_1 = \lg \left(\frac{A_{565}^0 - A_{671}^0}{A_{565} - A_{671}} - 1 \right) = \text{pH} - \text{p}K_a \quad (\text{Eq. S6})$$

Among them, A_{565} and A_{671} represent the absorption intensities of Rh-OH at 565 nm

and 671 nm at different pHs, respectively; A_{565}^0 and A_{671}^0 represent the absorption intensities of HB at 565 nm and 671 nm at different pHs, respectively. From the relationship between Y_1 and pH, the pKa of the Rh-OH was measured to be 7.5.

Fluorescence characteristics of Rh-OH responding to pH

Since the pKa of Rh-OH is 7.5, the system was approximated to have only the acidic configuration HB at pH 4.00. At this point, the fluorescence emission intensity at 670 nm versus 730 nm increased linearly with increasing concentration of HB, and the fluorescence contributions of different concentrations of acidic configurations HB at the wavelengths of 670 nm and 730 nm were y_1 and y_2 , as shown in Fig. S6A-S6C, respectively:

$$y_1 = 1115 x + 423.9 \quad (\text{Eq. S7})$$

$$y_2 = 868.8 x + 190.1 \quad (\text{Eq. S8})$$

At pH 11.00, it was approximated that only the base configuration B^- was present. At this point, the fluorescence emission intensity at 670 nm and 730 nm increased linearly with increasing B^- concentration, as shown in Fig. S6D-S6F, and the fluorescence contributions of different concentrations of the alkali conformation B^- to the 670 nm and 730 nm wavelengths were y_3 and y_4 , respectively:

$$y_3 = 80.37 x + 87.41 \quad (\text{Eq. S9})$$

$$y_4 = 620.8 x + 391.1 \quad (\text{Eq. S10})$$

Thus, at any pH, the fluorescence intensity of Rh-OH at 670 nm consisted of two components, y_1 of HB and y_3 of B^- . Meanwhile, the fluorescence intensity at 730 nm consisted of two components, y_2 of HB and y_4 of the B^- :

$$I_{670} = y_1 + y_3 \quad (\text{Eq. S11})$$

$$I_{730} = y_2 + y_4 \quad (\text{Eq. S12})$$

By substituting Eq. S7-S10 into Eq. S11 and Eq. S12, the equations for the concentration of the acidic configuration [HB] and the concentration of the alkaline configuration [B^-] versus the two-wavelength emission intensities, I_{670} and I_{730} , were obtained as follows:

$$[\text{HB}] = 9.97 \times 10^{-4} I_{670} - 1.29 \times 10^{-4} I_{730} - 0.435 \quad (\text{Eq. S13})$$

$$[B^-] = 1.767 \times 10^{-3} I_{730} - 1.376 \times 10^{-3} I_{670} - 0.323 \quad (\text{Eq. S14})$$

Therefore, the total concentration (c) of Rh-OH was calculated as follows:

$$c = 1.638 \times 10^{-3} I_{730} - 0.379 \times 10^{-3} I_{670} - 0.758 \quad (\text{Eq. S15})$$

DFT calculation of Rh-O-QL

All (TD)DFT calculations were carried out by Gaussian 16 and analyzed by Multiwfn 3.8 for Rh-O-QL, Rh-OH, and Rh-O⁻ [2-5]. M06-2X functional and 6-31+g(d,p) basis sets were utilized, meanwhile, the solvation effect of water was assessed by the SMD model.

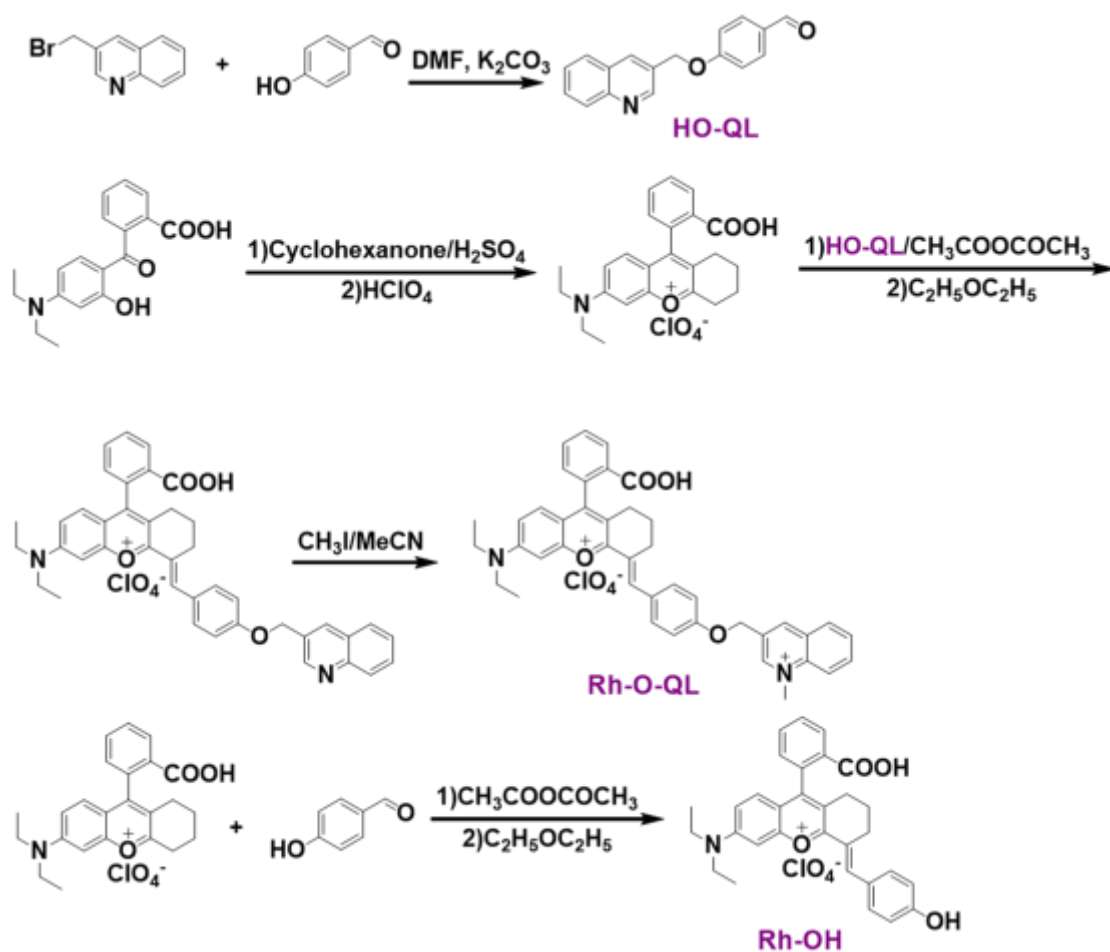
Cell Culture and Cytotoxicity Test

The 4T1 cells were obtained from the National Infrastructure of Cell Line Resource and cultured in DMEM medium with 10% fetal bovine serum (FBS) at 37°C and a 5% CO₂ atmosphere. The third to tenth generation cells after resuscitation were seeded on confocal dishes or 96 well plates and allowed to adhere for 24.0 h before being treated. For cytotoxicity assay, 4T1 cells (10⁶ cells/well) were incubated with different concentrations (0, 25, 50, 100, and 200 μM) of Rh-O-QL for another 12.0 h. Then the culture medium was changed and 10 μL CCK-8 solution was added to each well. After 3.0 h, the optical density at 450 nm of each well was recorded on a microplate reader. The absorbance of the cells in the medium was normalized and considered 100% viability in the control group. Meanwhile, different concentrations of Rh-O-QL were co-incubated with 4T1 cells for 12.0 h, followed by staining with Calcein AM/PI for 0.5 h.

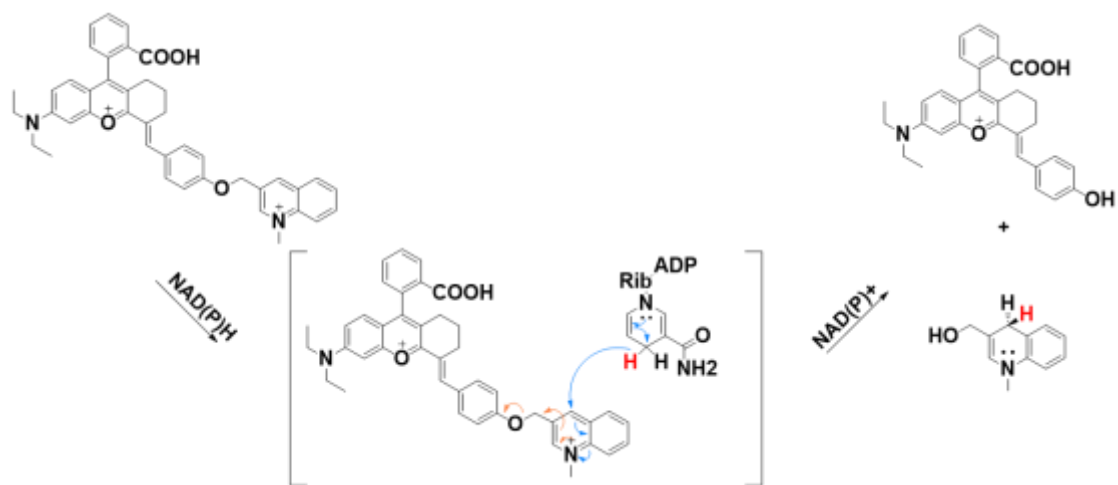
Fluorescence Imaging in living cells

For endogenous NAD(P)H imaging of 4T1 cells, the Rh-O-QL stock solution was added to the adherent cells to achieve a concentration of 50 μM Rh-O-QL, and time-dependent images were acquired after incubating for different times (0.25, 0.5, 1.0, 2.0, and 3.0 h). To obtain exogenous NAD(P)H images of 4T1 cells, the cells were cultured in different concentrations of NAD(P)H (0-1.0 mM) for 0.5 h and then stained with 50 μM Rh-O-QL for 1.0 h. For the colocalization assay, the cells were treated with 50 μM Rh-O-QL for 1.0 h, followed by being co-stained with 50 μM Rh-O-QL and 10 μM Mito-Tracker Green or 10 μM Lyso-Tracker Green for 0.5 h. To obtain NAD(P)H images in the energy metabolism of 4T1 cells, the cells were pre-treated with 0-20.0 mM glucose before incubating with 50 μM Rh-O-QL for 1.5 h. To obtain NAD(P)H images in the mitochondrial autophagy process, the cells were pre-treated with 10 μM CCCP for 0-5.0 h before incubating with 50 μM Rh-O-QL for 1.5 h.

All cells were washed with PBS three times after being stained. All images were collected on a confocal fluorescence microscope, using 600 nm excitation, 610-670 nm emission filters for Channel Acidic and 700-800 nm emission filters for Channel Alkaline in Rh-O-QL imaging, and 488 nm excitation, 500-640 nm emission filters in Mito-Tracker Green imaging, with 504 nm excitation, 515-580 nm emission filters in Lyso-Tracker Green imaging.



Scheme S1. Design of dual-response near-infrared dye molecule Rh-O-QL.



Scheme S2. Proposed mechanism of probe Rh-O-QL response to NAD(P)H.

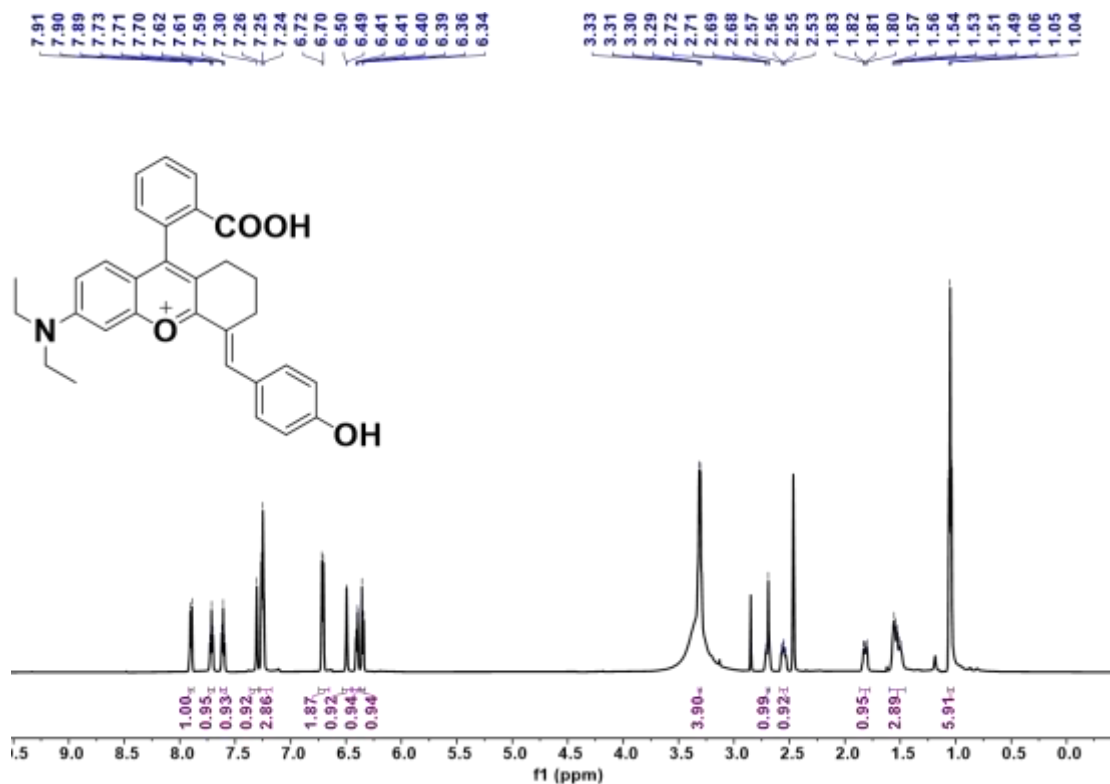


Figure S1. ¹H NMR spectra (600 MHz, DMSO-d₆) of compound Rh-OH.

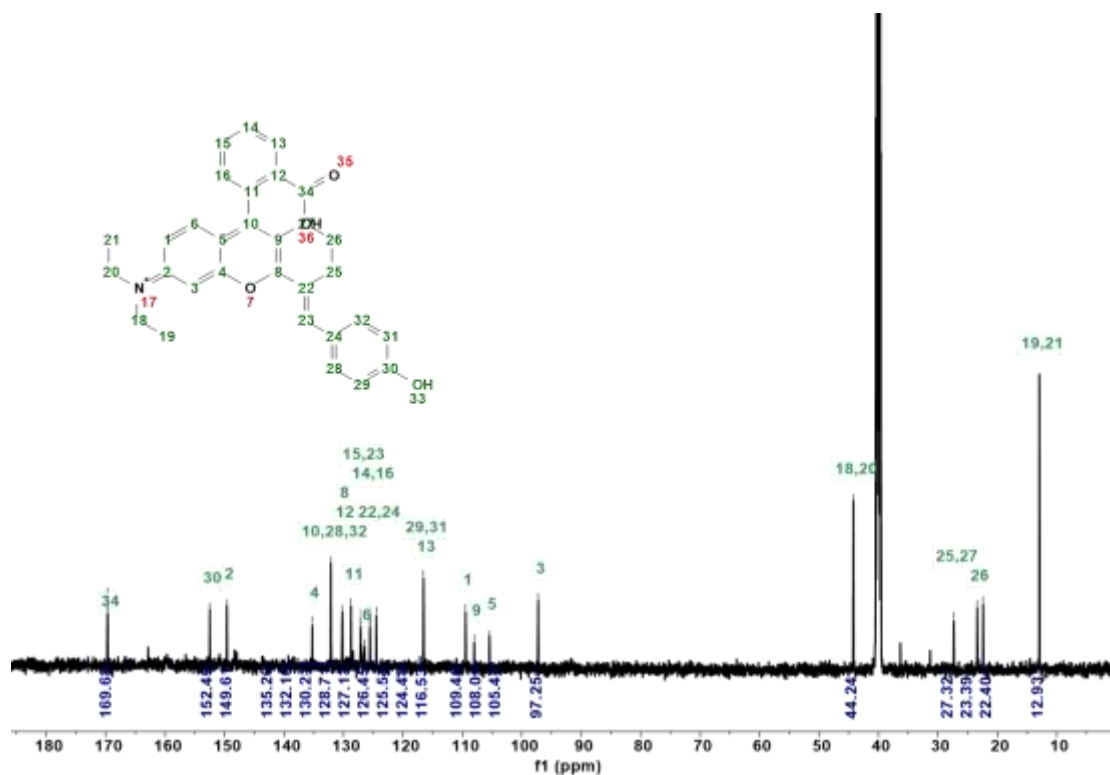


Figure S2. ¹³C NMR spectra (150 MHz, DMSO-d₆) of compound Rh-OH.

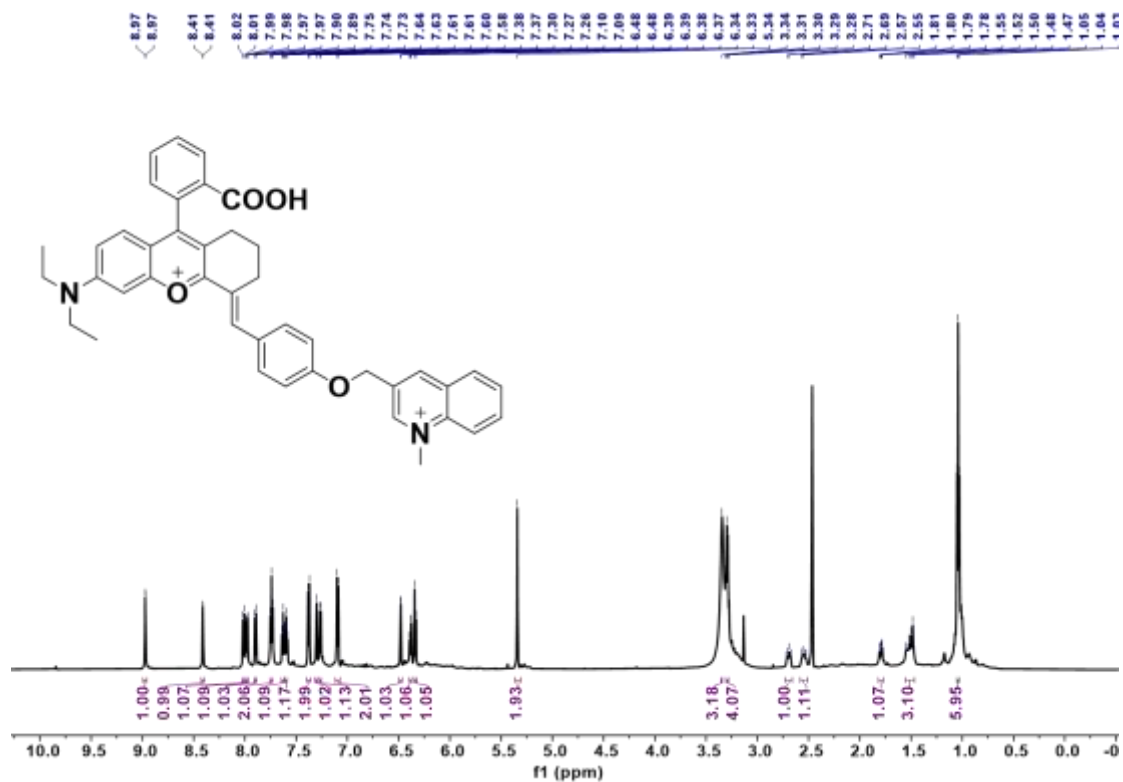


Figure S3. ^1H NMR spectra (600 MHz, DMSO- d_6) of compound Rh-O-QL.

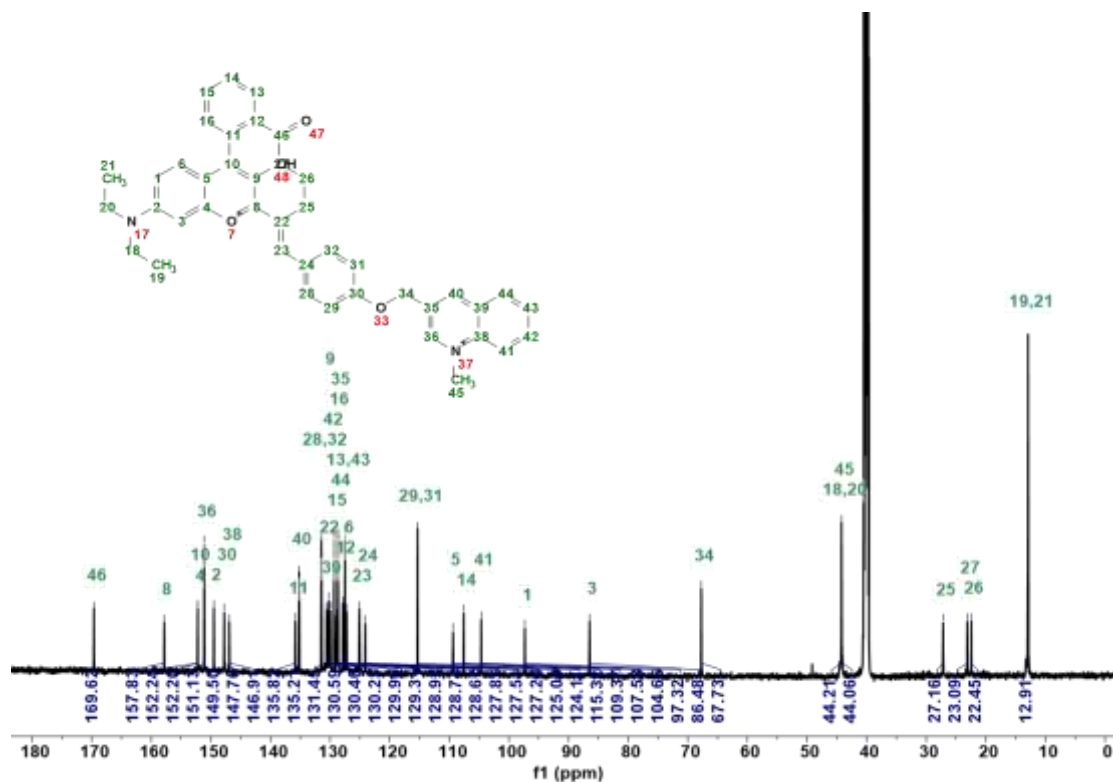


Figure S4. ^{13}C NMR spectra (150 MHz, DMSO- D_6) of compound Rh-O-QL.

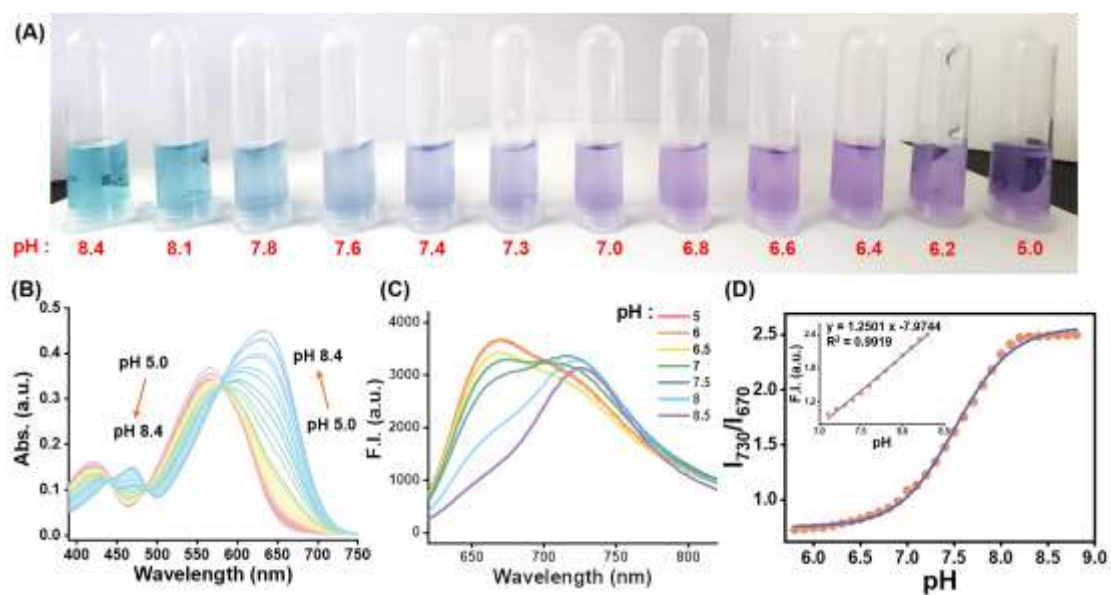


Figure S5. PH-responsive photophysical properties of Rh-OH. (A) Images of Rh-OH solution (20 μM) at different pH. (B) UV-vis absorption spectrum changes of Rh-OH (20 μM) at pH from 5.0 to 8.4. (C) Fluorescence-emission spectra of Rh-OH (20 μM) at pH from 5.0 to 8.5. (D) The trend of value of I_{730}/I_{670} with the change of pH.

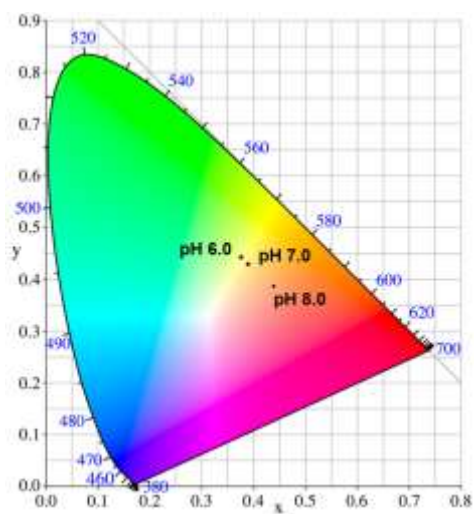


Figure S6. Chromaticity diagram of Rh-OH at different pH conditions (pH = 6.0, 7.0, 8.0)

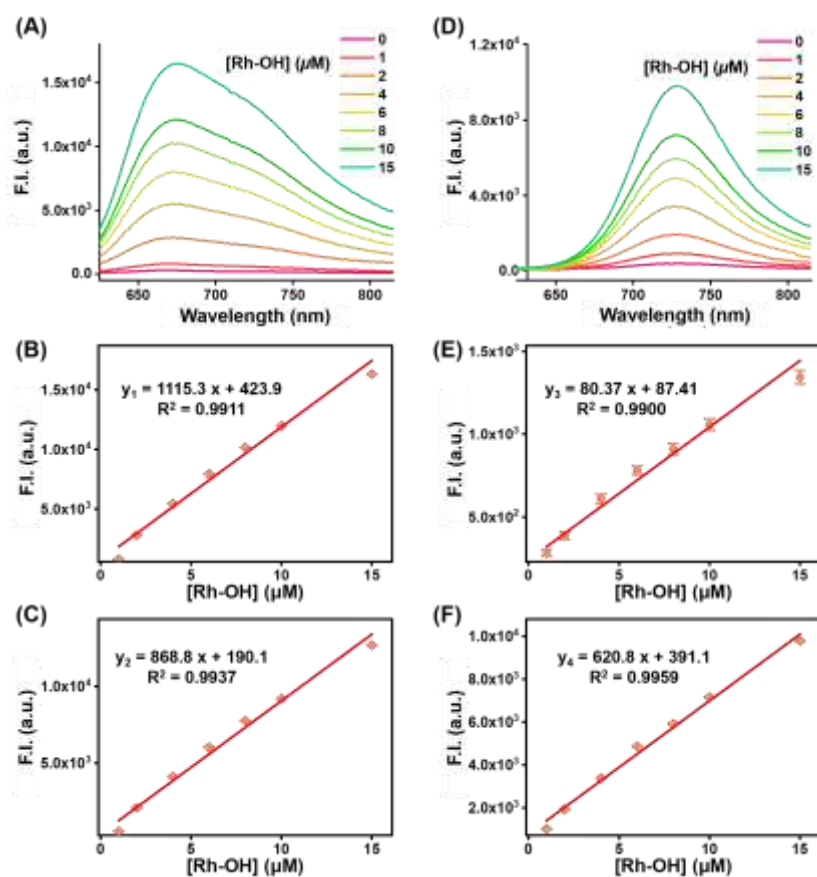


Figure S7. Fluorescence properties of acid-base configuration of Rh-OH. (A) Dose-dependent fluorescence spectrum of acidic Rh-OH (pH = 4.00). Line profile analysis for fluorescence intensity changes at 670 nm (B) and 730 nm (C) of acidic Rh-OH with concentrations. (D) Dose-dependent fluorescence spectrum of alkaline Rh-OH (pH = 10.00). Line profile analysis for fluorescence intensity changes at 670 nm (E) and 730 nm (F) of alkaline Rh-O⁻ with concentrations.

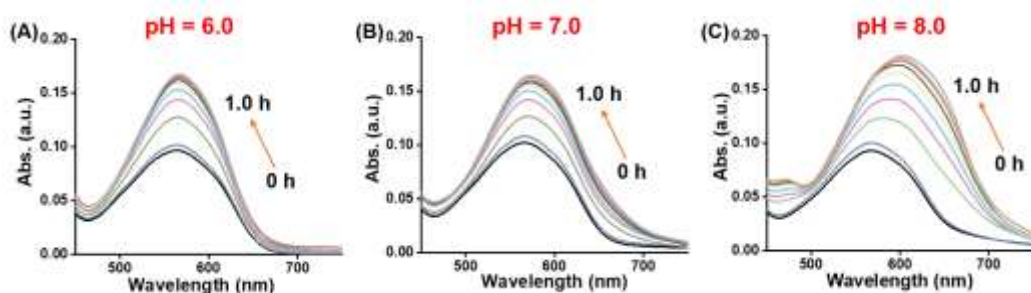


Figure S8. Time-dependent UV-vis absorption spectrum changes of Rh-DD-QL (20 μM) with NAD(P)H from 0-1.0 h at pH 6.0, 7.0 and 8.0, respectively.

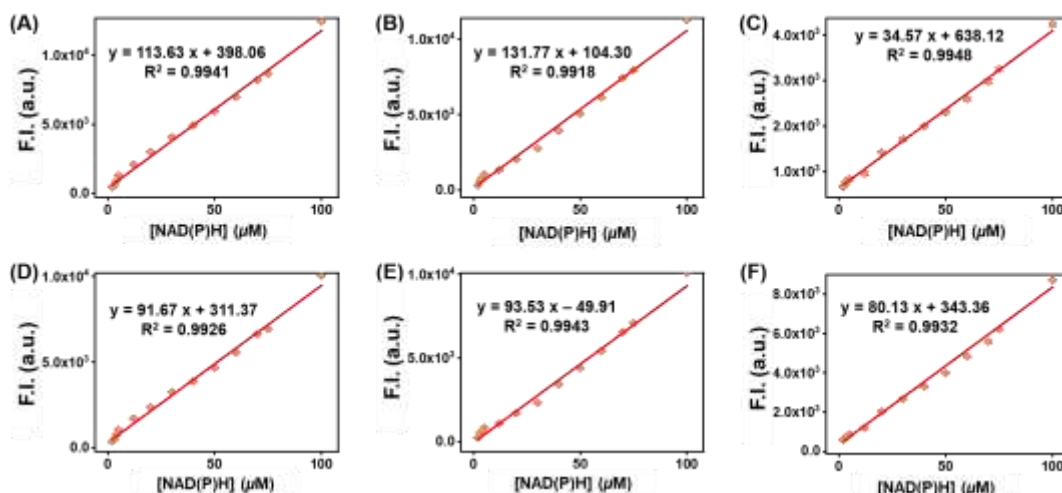


Figure S9. Line profile analysis for fluorescence intensity changes at 670 nm (A) and 730 nm (D) of Rh-O-QL with NAD(P)H concentrations at pH = 6.0. Line profile analysis for fluorescence intensity changes at 670 nm (B) and 730 nm (E) of Rh-O-QL with NAD(P)H concentrations at pH = 7.0. Line profile analysis for fluorescence intensity changes at 670 nm (C) and 730 nm (F) of Rh-O-QL with NAD(P)H concentrations at pH = 8.0.

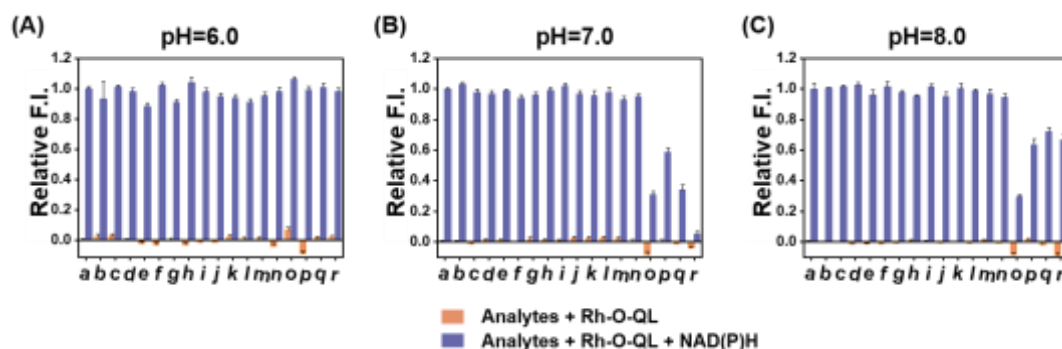


Figure S10. Relative fluorescence intensity of 20 μM Rh-O-QL in the presence of various analytes at pH = 6.0 (A), pH = 7.0 (B), pH = 8.0 (C). Analytes: (a) blank, (b) pyruvic acid, (c) ATP, (d) malic acid, (e) glucose, (f) sodium citrate, (g) ADP, (h) iso-citric acid, (i) FADH₂, (j) NAD(P)⁺, (k) α- Ketoglutaric acid, (l) inorganic cations (Na⁺, Al³⁺, Fe³⁺, K⁺, Ca²⁺), (m) organic phosphate (GTP, GDP, IMP, UTP, UDPG, AMP, CTP, GMP), (n) NaNO₂, (o) glutamic acid, (p) pancreatic enzyme, (q) serine, (r) lysine. Error bars represent standard deviation (n = 3).

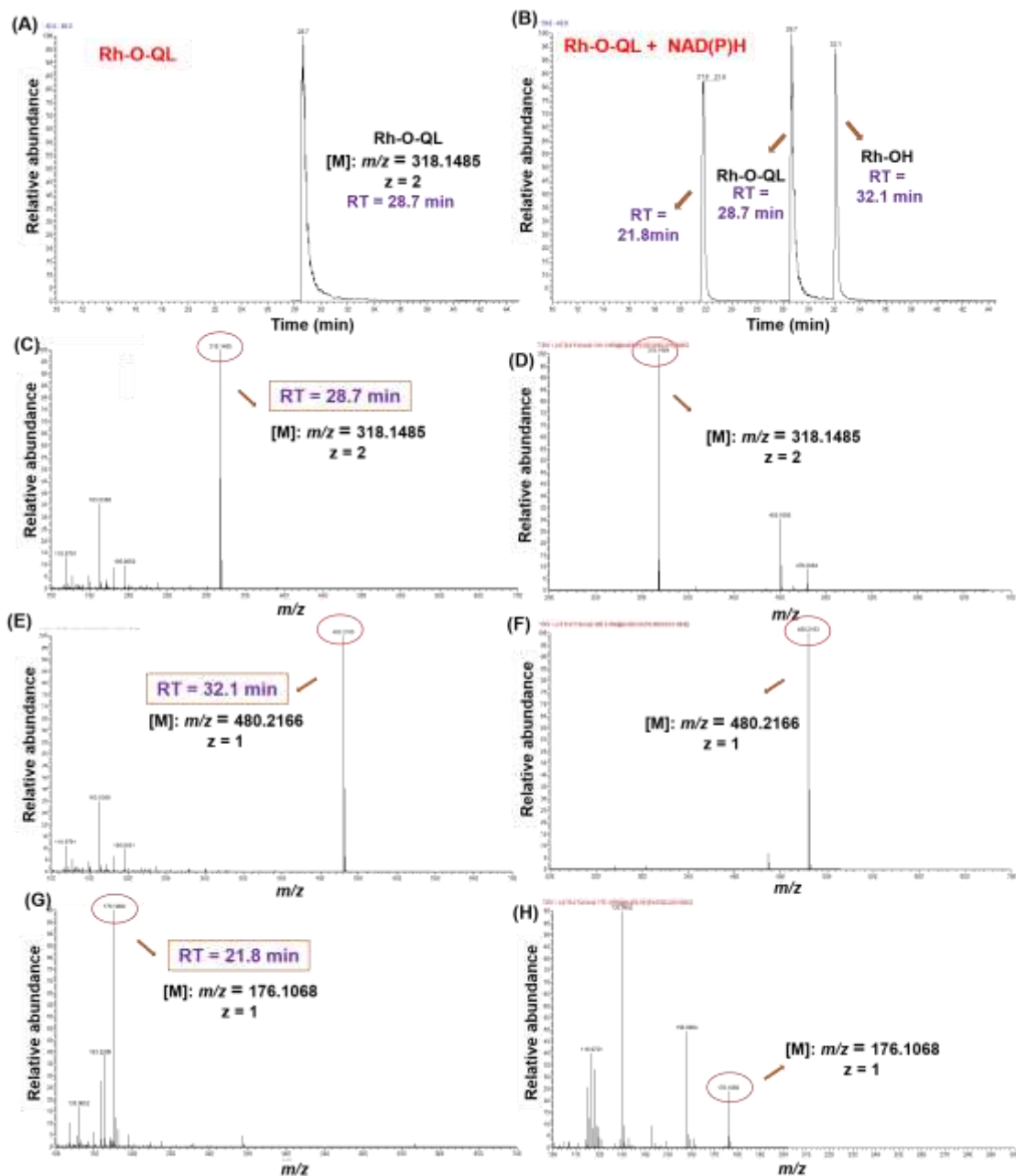


Figure S11. HPLC-MS spectrogram of Rh-O-QL before and after the addition of NAD(P)H. (A) HPLC-MS spectrogram of Rh-O-QL. (B) HPLC-MS spectrogram of Rh-O-QL + NAD(P)H. (C) Full scan MS spectrum for a retention time of 28.7 min in positive ion detection mode. (D) MS/MS spectrum of parent ion $m/z = 318.148$ ($z = 2$). (E) Full scan MS spectrum for a retention time of 32.1 min in positive ion detection mode. (F) MS/MS spectrum of parent ion $m/z = 480.216$. (G) Full scan MS spectrum for a retention time of 21.8 min in positive ion detection mode. (H) MS/MS spectrum of parent ion $m/z = 176.107$. Detection: UV-Vis (210, 254, 280, and 365 nm) detector. Flow rate: 0.3 mL/min. T: 30°C. Injection volume: 5 μ L. Mobile phase: 0.010-5 min: methanol-water, 5:95; 5-45 min: methanol-water, 5:95-95:5 (v/v); 45-50 min: methanol-water, 95:5; 50-55 min: methanol-water, 95:5-5:95.

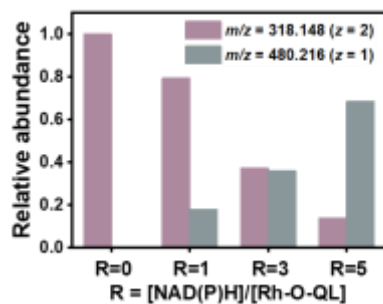


Figure S12. Relative abundance of Rh-O-QL ($m/z = 318.148$ ($z=2$), $RT = 28.7$ min) and the production of Rh-O-OH: Rh-OH ($m/z = 480.216$, $RT = 32.1$ min) after incubation with 0, 1, 3, and 5 equivalents NAD(P)H for 1.5 h.

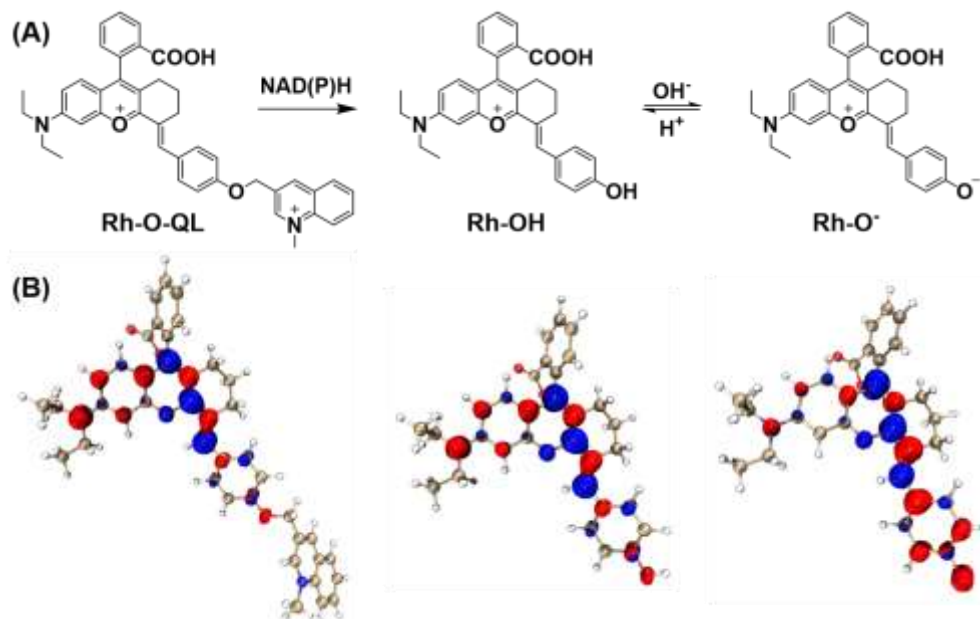


Figure S13. (A) Chemical structures, (B) Hole-electron distribution of Rh-O-QL, Rh-OH, and Rh-O⁻. The isosurface: 0.003 a.u. in value. Isosurface in red represents the hole charge carrier while blue represents the electron charge carrier.

Table S1. DFT calculation results of Rh-O-QL, Rh-OH, and Rh-O⁻.

	Excitation Energy (eV/nm)	Coulomb attractive energy (eV)	Transition electric dipole moment from S0 → S1	Oscillator strength
Rh-O-QL	1.936 / 640.27 (DFT) 1.851 / 670 (exp.)	3.65	4.85	1.116
Rh-OH	1.928 / 642.93 (DFT) 1.851 / 670 (exp.)	3.72	4.87	1.121
Rh-O⁻	1.686 / 735.34 (DFT) 1.699 / 730 (exp.)	3.73	5.87	1.425

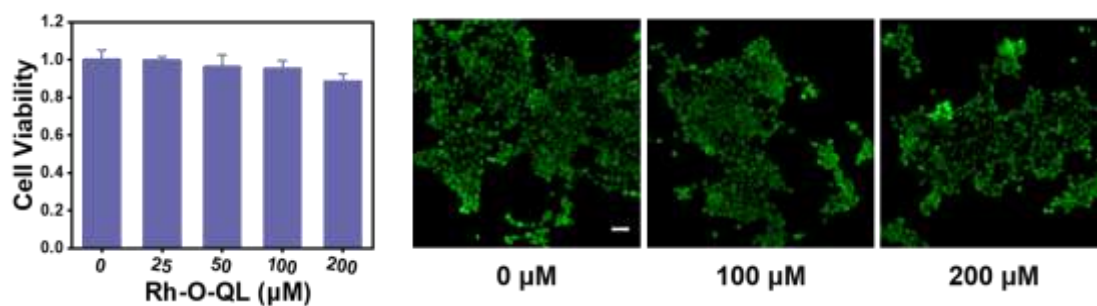


Figure S14. Cytotoxicity assays of probe Rh-O-QL. (A) Cell viability staining image of 4T1 cells incubated with 0, 100, and 200 μM Rh-O-QL for 12 h. (B) Relative viability of 4T1 cells incubated with various concentrations of Rh-O-QL for 12 h. Error bars represent standard deviation ($n = 3$). Scale bar: 100 μm.

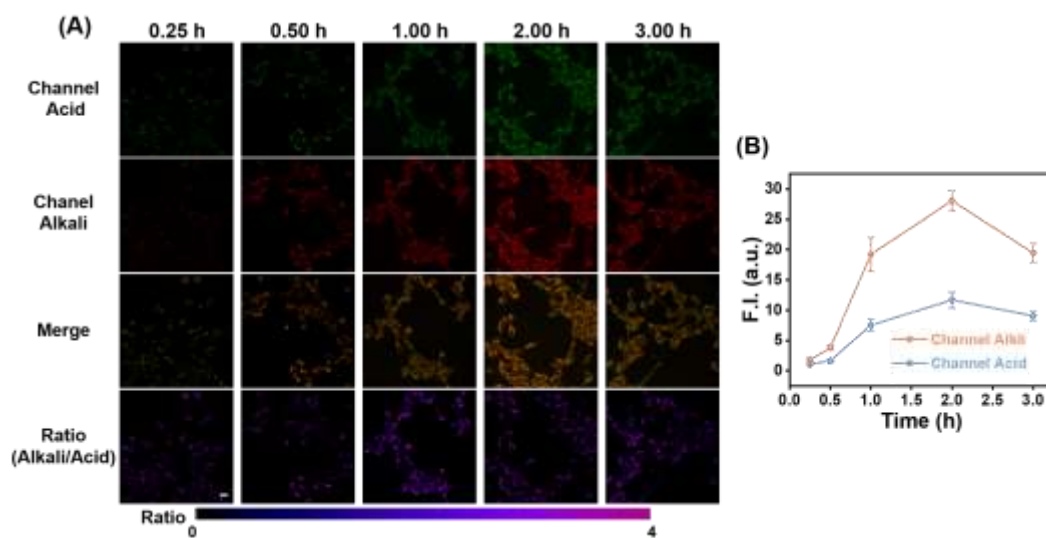


Figure S15. The time-dependence of cellular fluorescence images and the fluorescence intensity of 4T1 cells in the incubation of 0.25, 0.50, 1.00, 2.00, and 3.00 h with 50 μM Rh-O-QL, in Channel Acid (green pseudo color, 610-670 nm) and Channel Alkali (red pseudo color, 700-800 nm). Scale bar: 20 μm. Error bars represent standard deviation ($n = 3$).

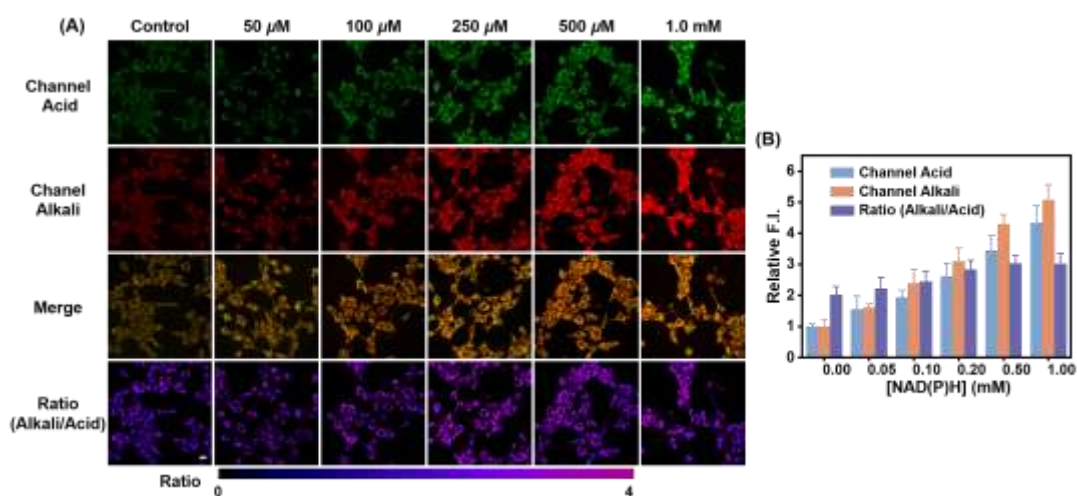


Figure S16. Fluorescence images of exogenous NAD(P)H 4T1 cells (pre-treated with NAD(P)H (0-1.0 mM, 30 min) and then stained with Rh-O-QL (50 μM, 1.5 h), in Channel Acid (green pseudo color, 610-670 nm) and Channel

Alkali (red pseudo color, 700-800 nm). Scale bars: 20 μ M. Further, the pictures were subjected to ImageJ quantification of fluorescence (B). Error bars represent standard deviation (n = 3)

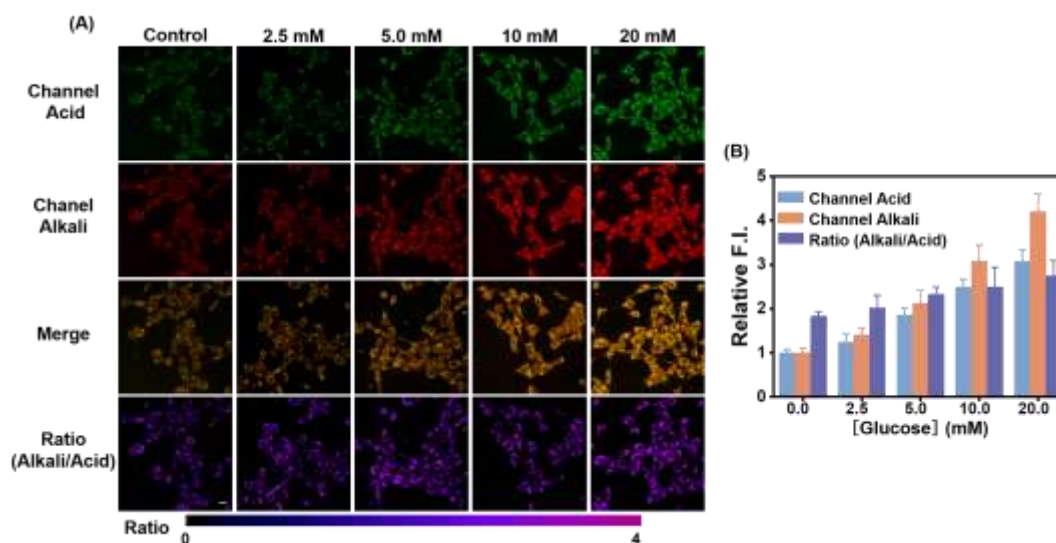


Figure S17. Fluorescence images of exogenous Glucose 4T1 cells (pre-treated with Glucose (0-20.0 mM, 30 min) and then stained with Rh-O-QL (50 μ M, 1.5 h), in Channel Acid (green pseudo color, 610-670 nm) and Channel Alkali (red pseudo color, 700-800 nm). Scale bars: 20 μ m. Further the pictures were subjected to ImageJ quantification of fluorescence (B). Error bars represent standard deviation (n = 3)

Reference

- [1] L. Guan, H. Sun, J. Xiong, W. Hu, M. Ding, Q. Liang, *Sens. Actuators B Chem.* 373 (2022) 132694.
- [2] M.J. Frisch, G.W. Trucks, H.B. Schlegel, G.E. Scuseria, M.A. Robb, J.R. Cheeseman, G. Scalmani, V. Barone, G.A. Petersson, H. Nakatsuji, X. Li, M. Caricato, A.V. Marenich, J. Bloino, B.G. Janesko, R. Gomperts, B. Mennucci, H.P. Hratchian, J.V. Ortiz, A.F. Izmaylov, J.L. Sonnenberg, Williams, F. Ding, F. Lipparini, F. Egidi, J. Goings, B. Peng, A. Petrone, T. Henderson, D. Ranasinghe, V.G. Zakrzewski, J. Gao, N. Rega, G. Zheng, W. Liang, M. Hada, M. Ehara, K. Toyota, R. Fukuda, J. Hasegawa, M. Ishida, T. Nakajima, Y. Honda, O. Kitao, H. Nakai, T. Vreven, K. Throssell, J.A. Montgomery Jr., J.E. Peralta, F. Ogliaro, M.J. Bearpark, J.J. Heyd, E.N. Brothers, K.N. Kudin, V.N. Staroverov, T.A. Keith, R. Kobayashi, J. Normand, K. Raghavachari, A.P. Rendell, J.C. Burant, S.S. Iyengar, J. Tomasi, M. Cossi, J.M. Millam, M. Klene, C. Adamo, R. Cammi, J.W. Ochterski, R.L. Martin, K. Morokuma, O. Farkas, J.B. Foresman, D.J. Fox, *Gaussian 16 Rev. C.01*, Wallingford, CT, 2016.
- [3] Z. Liu, T. Lu, Q. Chen, *Carbon* 165 (2020) 461-467.
- [4] T. Lu, *J. Chem. Phys.* 161 (2024) 082503.
- [5] T. Lu, F. Chen, *J. Comput. Chem.* 33 (2012) 580-592.